ChemComm

COMMUNICATION

View Article Online
View Journal | View Issue

Cite this: *Chem. Commun.*, 2015, **51**, 15418

Received 30th June 2015,
Accepted 24th August 2015

DOI: 10.1039/c5cc05370f

www.rsc.org/chemcomm

An ultra-sensitive hydrogen gas sensor using reduced graphene oxide-loaded ZnO nanofibers†

Zain Ul Abideen,[a] Hyoun Woo Kim*[b] and Sang Sub Kim*[a]

We developed a hydrogen sensor of reduced graphene oxide-loaded ZnO nanofibers. An extremely high response of about 866 at a low concentration of 100 ppb was obtained. The combined effect of the presence of rGO nanosheets and hydrogen-induced metallization of ZnO played a crucial role in enhancing the detection behavior.

Hydrogen (H_2) is a clean, efficient, and promising candidate for renewable energy sources that will overcome current challenges such as air pollution, global warming, and the global energy crisis. In this growing hydrogen economy, safety challenges involving hydrogen gas production, transportation, and storage require highly efficient, early and accurate detection of escaped or leaked H_2 gas. Therefore, rapid detection of H_2 gas at very low concentration is crucial to ensure safety at hydrogen facilities and during storage and usage.[1–3]

One-dimensional (1D) electrospun nanofibers (NFs) are renowned for their potential applications in chemical sensors mainly due to their large surface-to-volume ratios,[4] small dimensions compared to the Debye length, and web-like structures with a large number of nanograins exposed to the analyte gas. In addition, electrospun NFs can be easily produced on a large commercial scale at low cost due to the facile electrospinning process, with possible functionalization of their surfaces with target-specific receptor species and possible surface deposition of a catalyst to promote or inhibit specific reactions.[5]

Zinc oxide (ZnO) is one of the most common metal oxides that has been widely employed in chemical sensors because of its many appealing properties such as good conductivity,[6] low toxicity,[7] and good thermal stability.[6,7] More importantly, ZnO-based gas sensors have excellent selectivity to toxic, flammable, and explosive gases, particularly ethanol[8] and hydrogen.[9] In order to achieve the highest sensitivity and selectivity of ZnO, many efforts have been made using a variety of strategies, including addition of noble metals or oxide catalysts and manipulation of composition and operating temperature.[10]

Alternatively, graphene, a one-atom layer of sp^2-bonded carbon atoms, has recently been introduced as a promising sensor material due to its excellent electrical, thermal, and mechanical properties with a high surface area (2600 $m^2\ g^{-1}$).[11] The high charge mobility enables the detection of single molecules of gaseous analytes, with great potential to achieve ultra-high sensitivity.[12] Because pure graphene does not exhibit acceptable sensitivity to gas,[13] chemically reduced graphene oxide (rGO) has been used due to its reported high sensitivity to gas molecules such as NO_2,[12] NH_3,[14] and H_2,[15,16] presumably due to good adsorption sites.

With the expectation of better sensitivity due to the addition of rGO in metal oxide semiconductor-based gas sensors, we report a highly sensitive and selective H_2 sensor of rGO and ZnO nanofibers fabricated using a low-cost and versatile electrospinning process. To our knowledge, there have been no reports demonstrating the incorporation of rGO in electrospun ZnO NFs. The sensing results were characterized as a function of H_2 concentration and operating temperature. Furthermore, we compared the sensing behavior of rGO/SnO_2-based NFs to that of rGO/ZnO-based NFs. SnO_2 is widely known as one of the most useful and studied sensing materials to detect dangerous gases such as H_2.[17,18] With low-cost and simple fabrication of various kinds of nanostructures, SnO_2 can have a lot of room for further enhancement of sensing capabilities. The results show that the rGO/ZnO-based composite NF is a promising material system for the rapid and selective detection of H_2 gas. Experimental procedures are described in the ESI† (Text S1 and Fig. S1).[19,20]

The microstructure and morphology of NFs were analyzed using FE-SEM and TEM (Fig. 1). Fig. 1a and b demonstrate that calcination did not significantly change the morphology of the NFs. After calcination at 600 °C for 0.5 h in air at a heating rate of 0.5 °C min^{-1}, the synthesized NFs exhibited a regular structure with an average diameter of 190 nm and were composed of a large

[a] *Department of Materials Science and Engineering, Inha University, 100 Inha-ro, Nam-gu, Incheon 402-751, Republic of Korea. E-mail: sangsub@inha.ac.kr; Fax: +82-32-862-5546; Tel: +82-32-860-7546*

[b] *Division of Materials Science and Engineering, Hanayng University, 222 Wangsimni-ro, Seongdong-Gu, Seoul, 133-791, Republic of Korea. E-mail: hyounwoo@hanyang.ac.kr; Tel: +82-2220-0382*

† Electronic supplementary information (ESI) available. See DOI: 10.1039/c5cc05370f

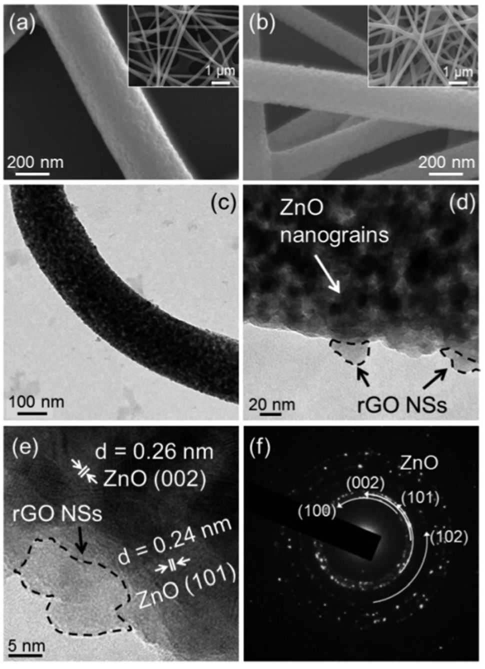

Fig. 1 SEM images of (a) as-spun and (b) calcined rGO-loaded ZnO composite NFs (Insets: low-magnification plane-view images). (c) Low-magnification TEM image of a calcined rGO-loaded ZnO composite NF. (d and e) TEM images of an enlarged surface region of (c). (f) Associated SAED pattern.

number of nanograins with an average size of 30 nm (Fig. 1b). The NFs and nanograins were uniform in size and shape. It is well known that the evolution of nanograins and the change in size modify the sensing properties of the NFs. The inset figure depicts the low-resolution SEM micrograph showing uniform and random distribution of the composite NFs on the Si/SiO_2 substrates.

The polycrystalline nature of the composite NFs in the presence of nanograins was confirmed by TEM examination (Fig. 1c–e) and was in good agreement with the SEM micrographs (Fig. 1b). Fig. 1e shows the magnified high-resolution TEM (HR-TEM) image of an enlarged surface region of an rGO-loaded ZnO composite NF. Several amorphous rGO nanosheets were observed on the surfaces of the nanograins, likely creating local heterojunctions with n-ZnO nanograins. The inter-planar distances of ZnO NFs were approximately 0.24 and 0.26 nm, respectively, which correspond to the (101) and (002) planes of the hexagonal ZnO phase (Fig. 1e). All the diffraction ring patterns were indexed to a hexagonal ZnO structure (JCPDS Card No. 89-1397) (Fig. 1f). The microstructure and morphology of rGO-loaded SnO_2 NFs were investigated by using FE-SEM and TEM (Fig. S2 and Text S2 in the ESI†).

In order to characterize the performance of the sensors composed of rGO-loaded ZnO composite NFs or rGO-loaded SnO_2 composite NFs, the sensors were exposed to a range of H_2 gas concentrations (100 ppb, 1 ppm, 5 ppm and 10 ppm) at various temperatures. Fig. 2, in conjunction with Fig. S3 (ESI†), summarizes the typical dynamic resistance curves and sensor responses of rGO/SnO_2 and rGO/ZnO composite NFs at 300, 350, 400, and 450 °C. The sensing behavior of both sensors was

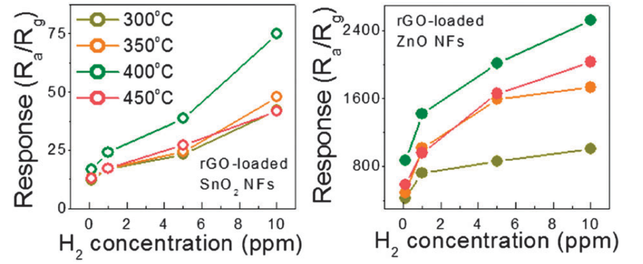

Fig. 2 Sensor responses of rGO/SnO_2 and rGO/ZnO composite NFs at 300, 350, 400, and 450 °C, depending on the H_2 concentration in the range of 0.1–10 ppm (open circles: rGO-loaded SnO_2 composite NFs; filled circles: rGO-loaded ZnO NFs).

similar to that of a typical n-type oxide semiconductor (*i.e.*, a decrease in resistance by a reducing gas) (Fig. S3, ESI†). The responses of both sensors monotonically increased with increasing H_2 gas concentration and temperature. Notably, rGO-loaded ZnO NFs exhibited greater responses than the rGO-loaded SnO_2 NFs at all temperatures, even to a trace amount of H_2 (100 ppb). The sensor responses of rGO-loaded SnO_2 NFs and rGO-loaded ZnO NFs were 74.8 and 2524.0, respectively, to 10 ppm of H_2 gas at 400 °C (Fig. 2 and Table S1 (ESI†)). Also, the rGO-loaded ZnO NFs were found to be extremely selectively sensitive to H_2 gas, in comparison to other gases, including NO_2, SO_2, O_2, CO, C_6H_6, and C_2H_5OH (Table S2 in the ESI†), demonstrating their potential use in the selective detection of H_2 in a harsh environment.

Fig. 3 shows the change in sensor responses of rGO-loaded SnO_2 NFs and rGO-loaded ZnO NFs with varying sensing temperatures in the range of 300–450 °C at a H_2 concentration of 10 ppm. The sensor responses of rGO-loaded ZnO NFs were 1007.5, 1731.6, 2524.0, and 2028.0 at 300, 350, 400, and 450 °C, respectively, whereas those of rGO-loaded SnO_2 NFs were 42.0, 47.8, 74.8, and 41.8, indicating that rGO-loaded ZnO NFs have significantly higher sensitivities than rGO-loaded SnO_2 NFs. In addition, the additional increase in the sensor response of rGO-loaded ZnO NFs with increasing temperature will be associated

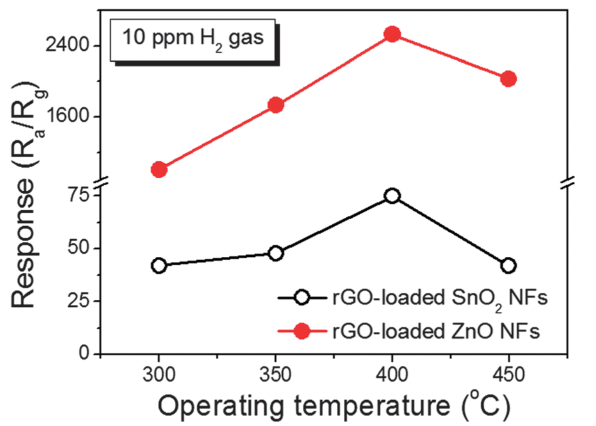

Fig. 3 Change in the sensor responses of rGO/SnO_2 and rGO/ZnO composite NFs upon varying the temperature from 300 to 450 °C at a H_2 concentration of 10 ppm.

with the enhancement of ZnO metallization at a higher temperature (Text S3 in the ESI†). The sensor response curves exhibited a bell-shaped behavior, with the maximum value at 400 °C. The possible reasons for the bell-shaped behavior are summarized in Text S4 (ESI†).

The sensor responses of rGO-loaded ZnO NFs were compared to those of rGO-loaded SnO_2, pure SnO_2, and pure ZnO NFs with respect to H_2 gas, wherein the H_2 concentration was fixed at 10 ppm (Fig. S4, ESI†). Not only the use of ZnO but also the introduction of rGO played crucial roles in enhancing the sensing behavior.

The main sensing mechanisms in ZnO NFs are schematically outlined in Fig. S5 (ESI†). First, there is resistance modulation due to the change in the radial thickness of the electron-depletion layer, underneath the surface. The depletion layer will be contracted and expanded, by the introduction and removal of H_2 gas, respectively. Second, excellent gas sensing characteristics of NFs were ascribed to the presence of grain boundaries, establishing the potential barriers and thus upward band bending at the grain boundaries in ambient air.[21] Upon introduction of target gas, H_2 molecules adsorb and react with chemisorbed oxygen in the ZnO grain boundaries, reducing the potential barriers and thus increasing the conductivity. While the resistance modulation through the introduction/removal of a target gas is a generally accepted mechanism for metal oxide NF-based gas sensors, the exceptionally high responses of the present NFs to H_2 gas indicate additional resistance modulation. Several studies have reported the creation of heterointerfaces between a metal oxide and graphene[19,22,23] for improving the sensing properties. Similarly, compared to pure SnO_2 NFs, the sensing responses of rGO-loaded SnO_2 NFs were significantly enhanced due to the presence of rGO.[9]

Additionally, the superior response of rGO-loaded ZnO NFs with respect to that of rGO-loaded SnO_2, in conjunction with the observation that pure ZnO NFs exhibit a superior sensor response to pure SnO_2 NFs, suggests that the interaction of H_2 with rGO-loaded ZnO noticeably affects the sensing behavior. Since the introduction of H_2 gas inevitably generates a metallic Zn layer along the rGO/ZnO heterojunctions (Text S5 in the ESI†), the energy band diagrams involving three phases should be considered (Fig. 4). From the differences in work functions, at equilibrium, the potential barriers will be generated not only at the rGO/Zn interfaces but also at the Zn/ZnO interfaces. First, the n-ZnO will become more n-type, by the transfer of electrons from metallic Zn. With the enlarged ZnO depletion region on the NF surface, the introduction/removal of H_2 will generate the relatively larger resistance modulation. Second, in ambient H_2, the potential barrier of rGO/Zn prevents the electron flow into rGO. Accordingly, the electrons in the ZnO region of sensor devices will not be lost to the rGO region. This will further decrease the resistance, which will be induced by the introduction of H_2 gas. Third, the rGO NSs will exert the spillover effect, enhancing the sensing behavior. The mechanisms involved in the improvement of sensing abilities of these sensors with respect to the ZnO/rGO heterointerfaces are described in more detail in Text S5 (ESI†). Based on our results, the extraordinary

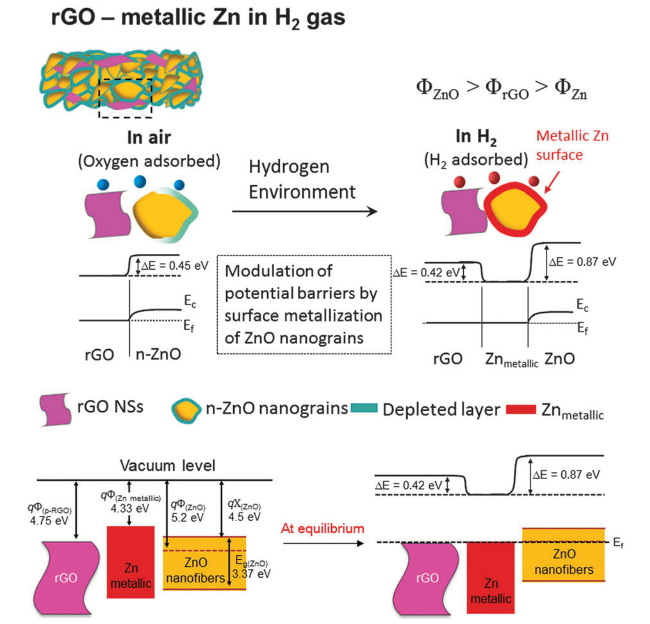

Fig. 4 Schematic illustration of the sensing mechanisms in which the surface of the ZnO nanograin is metallized.

improvement in the sensing properties of rGO-loaded ZnO NFs for H_2 is primarily due to the surface metallization effect (occurring in a H_2 atmosphere) combined with the creation of local heterojunctions. The possible reason for the strikingly superior response of rGO-loaded ZnO NFs in comparison to that of rGO-loaded SnO_2 is explained in detail in Text S6 (ESI†).

A comparison of ZnO-based H_2 sensors to findings of previous studies is shown in Table S3 in the ESI.† Although extraordinarily high sensor responses were observed from sensors consisting of SnO_2 thin films,[24,25] the H_2 concentration was in the range of 800–1000 ppm. Despite the importance of hydrogen sensor operation at low concentrations, there have been few studies on such sensors. The Bi_2S_3 nanowire-based sensors exhibited a room-temperature sensor response of 1.22 at 10 ppm.[26] B. Wang *et al.* reported a sensor response <0.5 at 10 ppm using SnO_2 nanowires.[27] We recently developed a ZnO NF sensor, showing a H_2 detection response of 63.8 at a very low concentration of 0.1 ppm. This striking enhancement in H_2 sensitivity was ascribed to the hydrogen-induced metallization on the surface of ZnO nanograins.[9]

This work presents the highest response to date to a very small concentration of H_2 with short recovery times. Experimental results suggest that rGO-loaded ZnO-based gas sensors can be applied when very low H_2 detection is required due to the combined effect of p-rGO and the semiconductor-to-metal transition effect of ZnO in a H_2 atmosphere. However, better responses with more rapid responses and recovery times at a relatively low temperature can be obtained by tuning the heterointerfaces between p-rGO and n-ZnO nanograins and through functionalization or electronic sensitization with palladium or platinum nanoparticles. This study is in progress and will be presented in the following reports.

In summary, uniformly-distributed rGO-loaded NFs with average diameters of 190 nm were synthesized through a low-cost electrospinning process. These rGO-loaded NFs had a polycrystalline nature due to the presence of a large number of nanograins, which were responsible for the additional resistance modulation at grain boundaries. The rGO nanosheets attached to the NFs greatly enhanced the sensing properties of the NFs by creating local heterointerfaces with the n-type nanograins and acted as electron acceptors. At 10 ppm, the rGO-loaded ZnO NFs exhibited a sensor response of approximately 2524. The rGO-loaded ZnO NFs exhibited excellent sensor responses (865.9) to a very low concentration of H_2 gas (100 ppb). These enhanced and extraordinary improvements in the sensing properties of rGO-loaded ZnO NFs were attributed to the combined effect of (i) the presence of rGO nanosheets and (ii) semiconductor-to-metal transition in a H_2 atmosphere. The present study provides a powerful insight into the enhancement of sensing abilities and selectivities due to the incorporation of rGO nanosheets and ZnO-based gas sensors for detecting trace amounts of H_2.

This work was supported by a National Research Foundation of Korea (NRF) grant funded by the Ministry of Education, Science and Technology (MEST) of Korea (no. 2012R1A2A2A01013899) and the International Research & Development Program of NRF funded by MEST (no. 2013K1A3A1A21000149).

Notes and references

1 W. J. Buttner, M. B. Post, R. Burgess and C. Rivkin, *Int. J. Hydrogen Energy*, 2011, **36**, 2462–2470.
2 C. S. Hsu, H. I. Chen, P. C. Chou, J. K. Liou, C. C. Chen, C. F. Chang and W. C. Liu, *IEEE Sens. J.*, 2013, **13**, 1787–1793.
3 T. Hübert, L. Boon-Brett, V. Palmisano and M. A. Bader, *Int. J. Hydrogen Energy*, 2014, **39**, 20474–20483.
4 J. Xu, N. Wu, C. Jiang, M. Zhao, J. Li, Y. Wei and S. X. Mao, *Small*, 2006, **2**, 1458–1461.
5 E. Comini and G. Sberveglieri, *Mater. Today*, 2010, **13**, 28–36.
6 W. Wang, H. M. Huang, Z. Y. Li, H. N. Zhang, Y. Wang, W. Zheng and C. Wang, *J. Am. Ceram. Soc.*, 2008, **91**, 3817–3819.
7 A. Baranowska-Korczyc, K. Fronc, L. Klopotowski, A. Reszka, K. Sobczak, W. Paszkowicz, W. Paszkowicz, K. Dybko, P. Dluzewski, B. J. Kowalski and D. Elbaum, *RSC Adv.*, 2013, **3**, 5656–5662.
8 Y. B. Zhang, J. Yin, L. Li, L. X. Zhang and L. J. Bie, *Sens. Actuators, B*, 2014, **202**, 500–507.
9 A. Katoch, S. W. Choi, H. W. Kim and S. S. Kim, *J. Hazard. Mater.*, 2015, **286**, 229–235.
10 C. W. Na, H. S. Woo, I. D. Kim and J. H. Lee, *Chem. Commun.*, 2011, **47**, 5148–5150.
11 G. Singh, A. Choudhary, D. Haranath, A. G. Joshi, N. Singh, S. Singh and R. Pasricha, *Carbon*, 2012, **50**, 385–394.
12 F. Schedin, A. K. Geim, S. V. Morozov, E. W. Hill, P. Blake, M. I. Katsnelson and K. S. Novoselov, *Nat. Mater.*, 2007, **6**, 652–655.
13 Y. Zheng, D. Lee, H. Y. Koo and S. Maeng, *Carbon*, 2015, **81**, 54–62.
14 J. D. Fowler, M. J. Allen, V. C. Tung, Y. Yang, R. B. Kaner and B. H. Weiller, *ACS Nano*, 2009, **3**, 301–306.
15 G. Lu, S. Park, K. Yu, R. S. Ruoff, L. E. Ocola, D. Rosenmann and J. Chen, *ACS Nano*, 2011, **5**, 1154–1164.
16 J. L. Johnson, A. Behnam, S. J. Pearton and A. Ural, *Adv. Mater.*, 2010, **22**, 4877–4880.
17 Y. L. Wang, X. C. Jiang and Y. N. Xia, *J. Am. Chem. Soc.*, 2003, **125**, 16176–16177.
18 L. Cheng, S. Y. Ma, X. B. Li, J. Luo, W. Q. Li, F. M. Li, Y. Z. Mao, T. T. Wang and Y. F. Li, *Sens. Actuators, B*, 2014, **200**, 181–190.
19 J. H. Lee, A. Katoch, S. W. Choi, J. H. Kim, H. W. Kim and S. S. Kim, *ACS Appl. Mater. Interfaces*, 2015, **7**, 3101–3109.
20 K. A. Alim, V. A. Fonoberov, M. Shamsa and A. Balandin, *J. Appl. Phys.*, 2005, **97**, 124313.
21 A. Tricoli, M. Righettoni and A. Teleki, *Angew. Chem., Int. Ed.*, 2010, **49**, 7632–7659.
22 S. Deng, V. Tjoa, H. M. Fan, H. R. Tan, D. C. Sayle, M. Olivo, S. Mhaisalkar, J. Wei and C. H. Sow, *J. Am. Chem. Soc.*, 2012, **134**, 4905–4917.
23 G. Neri, S. G. Leonardi, M. Latino, N. Donato, S. Baek, D. E. Conte, P. A. Russoe and N. Pinnad, *Sens. Actuators, B*, 2013, **179**, 61–68.
24 L. A. Patil, M. D. Shinde, A. R. Bari and V. V. Deo, *Sens. Actuators, B*, 2009, **143**, 270–277.
25 N. S. Baik, G. Sakai, N. Miura and N. Yamazoe, *Sens. Actuators, B*, 2000, **63**, 74–79.
26 K. Yao, W. W. Gong, Y. F. Hu, X. L. Liang, Q. Chen and L. M. Peng, *J. Phys. Chem. C*, 2008, **112**, 8721–8724.
27 B. Wang, L. F. Zhu, Y. H. Yang, N. S. Xu and G. W. Yang, *J. Phys. Chem. C*, 2008, **112**, 6643–6647.